J Eng Math (2021) 127:23
https://doi.org/10.1007/s10665-021-10118-2

On the performance of multilayered membrane filters

D. Fong · L. J. Cummings · S. J. Chapman · P. Sanaei

Received: 28 May 2020 / Accepted: 18 February 2021 / Published online: 20 March 2021

Abstract Multilayered membrane filters, which consist of a stack of thin porous membranes with different properties (such as pore size and void fraction), are widely used in industrial applications to remove contaminants and undesired impurities (particles) from a solvent. It has been experimentally observed that the performance of well-designed multilayer structured membranes is markedly better than that of equivalent homogeneous membranes. Mathematical characterization and modeling of multilayered membranes can help our understanding of how the properties of each layer affect the performance of the overall membrane stack. In this paper, we present a simplified mathematical model to describe how the pore-scale properties of a multilayered membrane affect the overall filter performance. Our results show that, for membrane stacks where the initial layer porosity decreases with depth, larger (negative) porosity gradients within a filter membrane are favorable for increasing throughput and filter lifetime, but at the expense of moderately poorer initial particle retention. We also found that the optimal layer thickness distribution that maximizes total throughput corresponds to a membrane stack with larger (negative) porosity gradients in which layer thickness increases slightly between successive layers in the depth of the membrane.

Keywords Depth filtration · Mathematical modeling · Multilayered membrane filters · Porosity-graded filter · Porous media flow

The views expressed in this article are D. Fong's own and not those of the U.S. Merchant Marine Academy, the Maritime Administration, the Department of Transportation, or the United States government.

D. Fong
Department of Mathematics and Science, U.S. Merchant Marine Academy, Kings Point, New York 11024, USA

L. J. Cummings
Department of Mathematical Sciences and Center for Applied Mathematics and Statistics, New Jersey Institute of Technology, Newark, NJ 07102-1982, USA

S. J. Chapman
Mathematical Institute, University of Oxford, Oxford OX2 6GG, UK

P. Sanaei (✉)
Department of Mathematics, New York Institute of Technology, New York, NY 10023-7692, USA
e-mail: psanaei@nyit.edu

1 Introduction

Membrane filters are used in many industrial engineering processes that require separating particles and contaminants of any given size from a fluid. Water purification [1], many separation processes in the biotech industry [2–5], treatment of radioactive sludge [6], and beer clarification [7] are just a few of the widespread applications. The details of the filtration in these applications may vary dramatically depending on the size of particles to be removed, the flow speed of the particle-laden solvent, the rigidity of the particles and so on; however, maintaining the desired separation control at a reasonable flow rate, using the least energy possible, is usually the ultimate goal. Therefore, for a given application, membrane filters with specific characteristics (such as flat or pleated [8,9], specific internal structure, specific pore sizes and shape [10–14], pore connectivity and distribution within the membrane [15]) may be needed.

A multilayered membrane consists of a stack of membranes, with different physical properties such as pore size and porosity, usually laminated at the layer junctions. Multilayered membranes are used widely in a variety of industrial applications, such as separation of cells or particles [15–17], or they can be combined to form the filtration support layers required in ultrafiltration, gas separation, and catalysis [18]. It has been demonstrated experimentally that a well-designed multilayer membrane performs better (according to a range of selected performance criteria) than a homogeneous membrane [19–22]. Mathematical characterization and modeling of multilayered membranes can help our understanding of how the properties of each layer affect the performance of the overall membrane stack.

Various models that attempt to analyze the performance of multilayered membrane filters have been formulated and examined to date. For instance, simple network models, in which the porous material is represented by a rectangular network where bonds and nodes represent pores and inter-pore connections (with each pore represented by a straight cylindrical capillary of specified length and diameter), respectively, have been studied by several authors. Such network models can quickly generate performance data, such as flux and particle retention characteristics, for a broad sweep of filter geometries (membrane microstructures). Early variants of such models [23–25] assume identical pores, but more recent versions [11,15] attempt to capture the depth variation of pore structure that is engineered in real membranes, allowing pore size and connectivity to be a function of depth through the membrane by adopting a layered structure, with changes in pore size/connectivity occurring at layer boundaries.

An important application of such models is in identifying optimal configurations for the pore microstructure, in terms of (for example) maximizing throughput of filtered fluid and filter lifetime, while removing an acceptable fraction of particles. Particles removed by the filter inevitably foul it, via three principal distinct fouling modes: (a) standard blocking or adsorptive fouling, in which particles smaller than the membrane pores are deposited or adsorbed within pores and shrink the pore radius; (b) blocking (complete or partial) of pores by large particles, which are "sieved" from the fluid; and (c) cake formation (once pores are blocked by large particles, other particles can accumulate on top of the membrane, forming a "cake" layer, adding additional resistance via a secondary porous layer on top) [2,12,26–29].

Many studies, both experimental and theoretical, have shown that a negative porosity gradient in the depth of the filter can improve filter efficiency [10,30–35] as measured by, for example, the total volume of filtrate fluid processed by the filter over its lifetime; the energy consumed in obtaining the filtrate; and also the level of contaminant remaining in the filtrate. This may be understood by noting that filter fouling necessarily is heaviest at the upstream side of the filter, where the feed suspension enters, thus this side needs to be more porous than the downstream side in order to deal with the heavier fouling burden. Filtration efficiency considerations are complicated by the frequent need for a very clean filtrate, which inevitably means that a large (downstream) portion of the filter membrane must remain nearly unfouled [15].

The goal of the present paper is to extend the scope of the work outlined above, by means of a novel continuum model of a multilayered filter that accounts for membrane internal geometry and porosity, and that allows fouling by both particle sieving and particle adsorption to operate simultaneously. The paper is laid out as follows: in Sect. 2 we introduce our mathematical model for filtration driven by specified pressure drop (the constant flux scenario is considered in an Appendix A). The model is nondimensionalized (Sect. 3), and sample simulations,

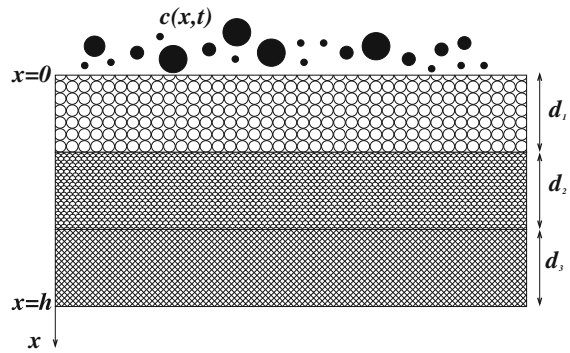

Fig. 1 Schematic of a multilayered filter, with 3 layers of thicknesses d_1, d_2, and d_3. Different shading patterns indicate different initial layer permeabilities

which demonstrate the important effects of membrane internal geometry and porosity, are presented in Sect. 4. Finally, we conclude in Sect. 5 with a discussion of our model and results in the context of real membrane filters, and of future modeling directions.

2 Model formulation

We consider filtration through a planar multilayer porous membrane perpendicular to the x-axis (see Fig. 1) with unidirectional Darcy flow of a "feed" suspension, assumed incompressible and Newtonian in the dilute suspension limit, through the membrane in the positive x-direction. The membrane properties and flow are assumed homogeneous in the plane of the membrane, but the permeability is depth-dependent (even if permeability is initially uniform, fouling will lead to nonuniformities over time, t), denoted by $k(x, t)$. We will model multilayered membranes by choosing the initial permeability $k(x, 0)$ to be a smoothed piecewise constant function, constant on each individual layer, but with rapid variations across short transition regions between layers.

The superficial Darcy velocity $\mathbf{u} = (u(x, t), 0, 0)$ within the membrane is then given in terms of the pressure p by

$$u = -\frac{k(x,t)}{\mu}\frac{\partial p}{\partial x}, \quad \frac{\partial u}{\partial x} = 0, \quad 0 \le x \le h, \tag{1}$$

where μ is the viscosity of the fluid and h is the total thickness of the multilayer membrane [36]. The membrane permeability $k(x, t)$ must be linked to membrane characteristics, which evolve in time due to fouling. Filtration commonly takes place under one of two scenarios: specified flux or pressure drop. In this paper, we mostly focus on the latter case, leaving a brief discussion of the constant flux scenario to the Appendix A. For constant applied pressure drop, the conditions applied at the upstream and downstream membrane surfaces, $x = 0$ and $x = h$, respectively, are

$$p(0, t) = p_0, \quad p(h, t) = 0. \tag{2}$$

We use the Kozeny–Carman model (see, for example [36]) to describe membrane permeability k as a function of the local membrane porosity or void fraction $\phi(x, t)$:

$$k = \frac{\chi\phi^3}{(1-\phi)^2}, \tag{3}$$

where χ is the Kozeny coefficient (with dimensions of length squared, as for permeability). Porosity $\phi(x, t) \in (0, 1)$ is the local pore volume fraction in any small membrane element at depth x and time t. The superficial Darcy velocity u is the fluid velocity averaged (locally, at depth x) over both membrane and pore volume, and differs from the

actual mean velocity of fluid within the pores (denoted by u_f and averaged over the pore cross-section at depth x). The membrane porosity links u_f and the superficial Darcy velocity u, within each layer of the filter stack, via

$$u = \phi u_\mathrm{f}. \tag{4}$$

The mass transport of the particles in the feed through the membrane stack may be described by an advection–diffusion–reaction equation

$$\frac{\partial(\phi c)}{\partial t} + \frac{\partial(u_\mathrm{f}\phi c)}{\partial x} = \mathcal{D}\frac{\partial^2(\phi c)}{\partial x^2} - f(c, u, \phi), \tag{5}$$

where $c(x, t)$ is the concentration of particles per unit volume of fluid in the membrane, $\mathcal{D}$ is the diffusion coefficient of particles in the feed suspension (here assumed constant), and $f(c, u, \phi)$ is the deposition function, which models how particles carried by the feed are deposited locally within the membrane and depends on the local particle concentration, Darcy velocity, and membrane porosity. Initially the membrane is clean, therefore the initial concentration of particles throughout the membrane is zero,

$$c(x, 0) = 0 \quad \text{for} \quad 0 < x < h. \tag{6}$$

At the membrane inlet, we assume the particle concentration is constant,

$$c(0, t) = c_0, \tag{7}$$

and conservation of mass implies that the mass flux of particles, $J = u_\mathrm{f}\phi c - \mathcal{D}\partial(\phi c)/\partial x$, must be continuous across $x = h$ [14,37], that is,

$$u_\mathrm{f}\phi c\Big|_{x=h^+} = \left[u_\mathrm{f}\phi c - \mathcal{D}\frac{\partial(\phi c)}{\partial x}\right]\Big|_{x=h^-} \Longrightarrow \frac{\partial(\phi c)}{\partial x}\Big|_{x=h} = 0. \tag{8}$$

In Sect. 3, we will discuss that the diffusion term is in fact always negligible compared to the advection and deposition terms, hence this second boundary condition (8) on the particle concentration will not be needed, since as $\mathcal{D} \to 0$, it becomes trivial.

The membrane porosity decreases as particles are deposited within the membrane on the pore walls. We assume this occurs at a rate proportional to the deposition function $f(c, u, \phi)$, hence

$$\frac{\partial\phi}{\partial t} = -\alpha f(c, u, \phi), \tag{9}$$

where α is a constant specific to the particular membrane/feed system, with dimensions of volume (inverse concentration). We solve Eq. (9) subject to a specified initial porosity profile,

$$\phi(x, 0) = \phi_0(x), \tag{10}$$

modeling the manufacturer-imposed variability of the membrane stack.

The model is closed by specifying the deposition function $f(c, u, \phi)$. We consider two distinct mechanisms for particle deposition: (i) adsorption (particles much smaller than the membrane pores are deposited onto the pore walls, shrinking pores and thus reducing the local porosity); and (ii) blocking (particles larger than the local membrane pore size get stuck and block the pore inlet). These two components will be modeled independently.

Our model assumes that there is no blockage at the layer interfaces (which might occur in practice due to imperfect layer contacts).

To propose a reasonable choice for $f(c, u, \phi)$, consider a membrane with spherical pores of radius r contained within cubes of fixed size D. For the adsorption, we note that the rate at which the particles arrive at the pore wall (and thus adhere) should be proportional to the local particle concentration and pore surface area, therefore we propose an adsorption rate proportional to $\phi^{2/3}c$ (note that for the proposed membrane structure, pore surface area scales with $\phi^{2/3}$, since $\phi \sim (r/D)^3$). In this model, we assume that adsorption simply requires that small particles in the vicinity of the wall deposit onto it. The rate at which this happens is assumed to depend primarily on the local concentration, independently of the local flow velocity. For blocking we require a large particle, bigger than the local pore size, to arrive and block the pore from above, hence we anticipate blocking to proceed at a rate proportional to the local advective flux of particles uc (large particles can either pass through a pore or they cannot: the more that pass a location the greater the blocking rate). Noting that pore radius scales with $\phi^{1/3}$, with the above assumptions blocking will also be proportional to $(1-\phi^{1/3})$ (smaller pores are more readily blocked). Hence, the blocking term is proportional to $u(1-\phi^{1/3})c$, and the deposition function $f(c, u, \phi)$ is taken as

$$f(c,u,\phi) = \underbrace{\bar{\lambda}\phi^{2/3}c}_{\text{adsorption}} + \underbrace{\bar{\delta}u(1-\phi^{1/3})c}_{\text{blocking}}, \tag{11}$$

where $\bar{\lambda} \geq 0$ is the average adsorption rate of particles, relating to the physics of the attraction between particles and pore wall; and $\bar{\delta} \geq 0$ is the average blocking coefficient, with dimensions of inverse length (in the absence of adsorption, $\bar{\delta}^{-1}$ gives a measure of the penetration depth of blocking particles into the membrane). The model assumes implicitly that particle sizes are uniformly distributed, and that all particles can enter the membrane, thus can be deposited within it by either adsorption or blocking fouling modes. According to the proposed model, blocking will dominate at high fluxes, while adsorption is more important in a low-flux scenario. The effect of changing porosity on the blocking behavior is inherent in the model. As pore constriction occurs and membrane resistance increases, the mean velocity of fluid within pores decreases. The changes in fluid velocity and porosity are both reflected in the blocking model, as explained by Eqs. (5)–(11).

3 Nondimensional model

We nondimensionalize the model (1)–(11) to reduce the number of parameters and to enable us to estimate the relative importance of the terms. We set

$$x = hx^*, \quad p = p_0 p^*, \quad (u, u_\mathrm{f}) = \frac{p_0\chi}{h\mu}(u^*, u_\mathrm{f}^*), \quad c = c_0 c^*, \quad k = \chi k^*, \quad t = \frac{h\mu}{c_0 p_0 \alpha \bar{\delta}\chi} t^*, \tag{12}$$

where starred variables are dimensionless. The spatial variable is scaled by the membrane thickness, h. We scale pressure by the specified pressure drop across the membrane, p_0, and the velocity scale then emerges from Darcy's law (1). Cross-sectionally averaged particle concentration is scaled by its value at the upstream membrane surface, c_0 (assumed constant); and permeability is scaled using a representative permeability value for the unused membrane, χ (see (3)). Note that there are two timescales in the problem: a short timescale, $h^2\mu/(p_0\chi)$, based on the flow transit time across the membrane, and a longer timescale, $h\mu/(c_0 p_0 \alpha\bar{\delta}\chi)$, on which particle deposition occurs (see (9) and (11)). Since our investigation primarily concerns the long-time fouling process resulting from particle deposition, we opt to scale the time variable by this timescale, $h\mu/(c_0 p_0 \alpha\bar{\delta}\chi)$; the flow adapts quasi-statically to the changing porosity. Dropping the stars, the dimensionless model in the multilayered membrane $0 \leq x \leq 1$ becomes

$$u = -k\frac{\partial p}{\partial x}, \quad \frac{\partial u}{\partial x} = 0, \tag{13}$$

$$k = \frac{\phi^3}{(1-\phi)^2}, \tag{14}$$

$$u_\mathrm{f} = \frac{u}{\phi}, \tag{15}$$

$$T_\mathrm{B}\frac{\partial(\phi c)}{\partial t} + u\frac{\partial c}{\partial x} = \mathrm{Pe}^{-1}\phi\frac{\partial^2 c}{\partial x^2} - \lambda\phi^{2/3}c - \delta u(1-\phi^{1/3})c, \tag{16}$$

$$\frac{\partial \phi}{\partial t} = -\frac{\lambda}{\delta}\phi^{2/3}c - u(1-\phi^{1/3})c, \tag{17}$$

where $T_\mathrm{B} = c_0\alpha h\bar{\delta}$ expresses the ratio of the advective particle transport timescale to that of the particle blocking, $\mathrm{Pe} = p_0\chi/(\mathcal{D}\mu)$ is the Peclet number associated with the particle diffusion, $\lambda = (h^2\bar{\lambda}\mu)/(p_0\chi)$ measures the relative rates of particle adsorption to advective particle transport, $\lambda/\delta = (h\bar{\lambda}\mu)/(p_0\bar{\delta}\chi)$ is a measure of the relative rates of particle adsorption and particle blocking, and $\delta = h\bar{\delta}$ is the dimensionless blocking coefficient.

Typical dimensional parameter values (where known) are given in Table 1, and dimensionless parameters are summarized in Table 2. Most of the parameters in Table 1 (such as χ, α, $\bar{\lambda}$, and $\bar{\delta}$) depend on physical characteristics of the filter membrane and feed solution, which vary from one application to another. Note that, in the absence of detailed experimental data, several model parameters are unknown, and we assign a range of values to be investigated to determine the optimal filtration regime.

In this work, we consider plausible filtration regimes where particle blocking and particle diffusion occur at much slower rates than the advective particle transport. In particular, we consider the limit $T_\mathrm{B} \ll 1$ and $\mathrm{Pe} \gg 1$ [38,39]. Hence the unsteady and diffusive terms may be neglected in Eq. (16), which then reduces to

$$u\frac{\partial c}{\partial x} = -\lambda\phi^{2/3}c - \delta u(1-\phi^{1/3})c. \tag{18}$$

We note that other limits may be physically relevant, depending on the application, but involve solving a more complex system with one or two additional parameters to be determined.

Equations (13)–(15) and (17)–(18) are solved subject to boundary and initial conditions:

$$p(0,t) = 1, \quad p(1,t) = 0, \quad c(0,t) = 1, \quad \phi(x,0) = \phi_0(x), \tag{19}$$

which are derived from the dimensional equivalents (2), (7), and (10) earlier. Integrating Eq. (13) and imposing boundary conditions (19) gives the pressure p and superficial Darcy velocity u as

$$p = u\int_x^1 \frac{(1-\phi)^2}{\phi^3}\,\mathrm{d}x', \qquad u = \left(\int_0^1 \frac{(1-\phi)^2}{\phi^3}\,\mathrm{d}x'\right)^{-1}, \tag{20}$$

hence, from (15), the cross-sectionally averaged (across the pore) fluid velocity

$$u_\mathrm{f} = \left(\phi\int_0^1 \frac{(1-\phi)^2}{\phi^3}\,\mathrm{d}x'\right)^{-1}. \tag{21}$$

Substituting (20) into (18) then integrating and applying (19) yields

$$c = \exp\left[-\int_0^x \left(\lambda\phi^{2/3}\int_0^1 \frac{(1-\phi)^2}{\phi^3}\,\mathrm{d}x' + \delta(1-\phi^{1/3})\right)\mathrm{d}x''\right]. \tag{22}$$

Table 1 Dimensional parameter values (Venkateshwaran, Private Communication, 2017; see also [40])

Parameter	Description	Typical value and units
h	Membrane thickness	10^{-4} m
μ	Viscosity of feed	10^{-3} kg m^{-1} s^{-1}
p_0	Pressure drop across membrane	Depends on application; here 10^5 kg m^{-1} s^{-2} used
χ	Kozeny coefficient (characteristic membrane permeability)	Depends on application; here 10^{-16} m^2 used
c_0	Total concentration of particles in feed suspension	Depends on application; 10^{-3} mol m^{-3}
$\mathcal{D}$	Diffusion coefficient of particles in feed suspension	10^{-11} m^2 s^{-1}
α	Pore shrinkage coefficient, see (9)	Unknown (depends on characteristics of membrane and feed suspension); m^3 mol^{-1}
$\bar{\lambda}$	Average adsorption rate of particles, see (11)	Unknown (depends on characteristics of membrane and feed suspension); s^{-1}
$\bar{\delta}$	Blocking coefficient, see (11)	Unknown (depends on characteristics of membrane and feed suspension); m^{-1}

The system thus reduces to Eq. (22), plus a single differential equation for the porosity, which is obtained by substituting (20) into (17),

$$\frac{\partial \phi}{\partial t} = -\left[\frac{\lambda}{\delta}\phi^{2/3} + \left(\int_0^1 \frac{(1-\phi)^2}{\phi^3}\,\mathrm{d}x'\right)^{-1}(1-\phi^{1/3})\right]c, \tag{23}$$

with c given by (22), to be solved subject to the initial condition

$$\phi(x,0) = \phi_0(x). \tag{24}$$

For future reference, we note that the flux in our model is directly proportional to the averaged Darcy velocity, therefore we define our dimensionless filtrate flux $q(t)$ and throughput $v(t)$ as

$$q(t) = u(0,t), \quad v(t) = \int_0^t q(t')\mathrm{d}t'. \tag{25}$$

These quantities will be used later in evaluating the performance of model multilayer filter membranes.

4 Results

We present sample results from our model (20)–(24) described in Sect. 3, in which we consider a number of relevant cases. In Sect. 4.1, we show preliminary results that illustrate how different choices of initial porosity profiles, $\phi(x,0) = \phi_0(x)$, modeling a multilayered membrane stack, can prolong or shorten the life span of the filter. In Sect. 4.2, we focus on the commonly considered case of filters whose initial porosity $\phi_0(x)$ decreases with depth (negative porosity gradient) and study the effect of membrane properties (such as particle adsorption, particle

Table 2 Dimensionless parameter definitions and range of values used

Parameter	Formula and description	Typical value
ϕ_0	Initial average porosity (void fraction)	0.5–0.7
Pe	$(p_0\chi)/(\mathcal{D}\mu)$ Ratio of advective and diffusive particle transport timescales (Peclet number)	Assumed asymptotically large
λ	$(h^2\bar{\lambda}\mu)/(p_0\chi)$ Ratio of rates of particle adsorption and advective particle transport (deposition coefficient)	Unknown; values in range 0.01–4 used
δ	$h\bar{\delta}$ Blocking coefficient (δ^{-1} measures penetrative potential of blocking particles in depth of membrane)	Unknown; values in range 2–16 used
λ/δ	$(h\bar{\lambda}\mu)/(p_0\bar{\delta}\chi)$	Unknown; values in range 10^{-2}–1 used
T_B	$c_0 h\alpha\bar{\delta} = c_0\alpha\delta$ Ratio of rates of pore-blocking and advective particle transport	Assumed asymptotically small

blocking, and membrane thickness) on filtration performance. Finally, in Sect. 4.3, we consider simple optimization of negative porosity gradient filters by varying selected design parameters such as the number of layers in the filter stack, the initial porosity of each layer in the stack, and the thicknesses of the individual layers.

From Darcy's law, the local membrane resistance is inversely proportional to permeability k (see (13)). We may define a dimensionless averaged membrane resistance, $r(t)$, as

$$r(t) = \int_0^1 \frac{\mathrm{d}x}{k(x,t)} = \int_0^1 \frac{(1-\phi(x,t))^2}{\phi(x,t)^3}\,\mathrm{d}x. \tag{26}$$

In order to make a meaningful comparison between different membrane structures, we compare results for initial porosity profiles $\phi(x,0)$ that give the same initial net membrane resistance $r_0 = r(0)$. Many alternative comparisons could be made: one could, for example, choose to fix the initial average membrane porosity. Ultimately our choice of fixing initial net resistance was made on the basis that all such membranes initially have the same energetic requirements, and therefore an important question is how these initially equivalent membranes compare over long filtration durations. As we will see, different initial porosity profiles with the same initial resistance evolve differently over time, so that resistances (and thus energetic requirements) at later times differ.

Briefly, our numerical solution scheme is as follows: Given an initial porosity profile $\phi_0(x) = \phi(x,0)$, we use trapezoidal quadrature to calculate the Darcy velocity u in (20). We then substitute for u in Eq. (22) to solve for the particle concentration c, again using trapezoidal quadrature. To account for the nonlinearity in the porosity Eq. (23), the porosity ϕ is calculated at the subsequent time step using an implicit Backward Euler method. This process is then repeated until the membrane becomes impermeable and the flux through it falls to zero at final time $t = t_f$ (when the Darcy velocity $u \to 0$). A convergence test was carried out to ensure that the first-order scheme converges as expected as the step size $\Delta t \to 0$.

4.1 Three-layer membranes

To gain insight into our model and the effect of layering, we first consider a membrane composed of three equal-thickness layers of different initial porosities, stacked on top of each other. While it is known empirically that filters whose initial porosity profile decreases with depth give superior filtration performance, for a more complete illustration of model behavior we also consider cases where initial porosity is monotonically increasing with depth; any combination of increasing or decreasing porosity between two successive layers; and initially uniform porosity. We present preliminary results for five different membrane stacks, modeled by the following choices of initial porosity profiles:

$$\phi(x,0) = \begin{cases} \phi_1(x,0) = 0.5289, \\ \phi_2(x,0) = 0.6350 - 0.1\tanh(400(x-0.33)) - 0.1\tanh(400(x-0.66)), \\ \phi_3(x,0) = 0.6326 + 0.1\tanh(400(x-0.33)) + 0.1\tanh(400(x-0.66)), \\ \phi_4(x,0) = 0.6424 - 0.1\tanh(400(x-0.33)) + 0.1\tanh(400(x-0.66)), \\ \phi_5(x,0) = 0.4947 + 0.1\tanh(400(x-0.33)) - 0.1\tanh(400(x-0.66)), \end{cases} \tag{27}$$

illustrated in Fig. 2. Each of these initial porosity profiles represent membrane stacks with the same initial net (dimensionless) resistance $r_0 = 1.50$ (the first, ϕ_1, may be considered to model a stack of three identical uniform membranes). However, the modeled membrane stacks have different initial average porosities[1], $\phi_{i,\text{avg}}(0)$: $\phi_{2,\text{avg}}(0) = 0.6350$, $\phi_{3,\text{avg}}(0) = 0.6326$, $\phi_{4,\text{avg}}(0) = 0.5757$, and $\phi_{5,\text{avg}}(0) = 0.5614$.

We simulate our model (20)–(24) for the initial porosity profiles of (27) with $\lambda = 1$ and $\delta = 8$. Figure 2a–e shows the evolving porosity profile $\phi(x,t)$ and the concentration of particles $c(x,t)$ within the feed as it passes through the membrane, for each of the five different membrane stacks, at various times throughout the evolution. Figure 2f shows the cross-sectionally averaged fluid velocity u_f for the initial porosity profile ϕ_2 (initial porosity decreasing in membrane depth). For all cases porosity decreases in time throughout the membrane filter due to fouling, with the most rapid reduction in $\phi(x,t)$ near the membrane inlet, reflecting the fact that the filter fouls primarily at the upstream side where the particle concentration in the feed is highest, while the downstream portions of the membrane remain minimally used for particle removal. This is especially true of membranes whose initial porosity is monotonically increasing with depth, exemplified here by ϕ_3. For cases where initial porosity decreases between two successive layers, specifically Fig. 2b (porosity decreases between layers 1 and 2, and again between layers 2 and 3), 2d (porosity decreases between layers 1 and 2), and Fig. 2e (porosity decreases between layers 2 and 3), the temporal decrease in porosity at the top of the downstream layer is much more rapid than for cases where porosity increases between successive layers. This difference in behavior is due primarily to the effect of the blocking term in our model (see Eq. (11) and its dimensionless equivalent equation (17)), and may be interpreted as modeling the physical phenomenon by which some particles are small enough to pass through the larger pores in the upstream layer, but too large to penetrate deep into the less porous layer downstream. The corresponding pore fluid velocity for one such decreasing porosity case (Fig. 2b) is shown in Fig. 2f, and is entirely consistent with the spatial and temporal behavior of ϕ: initially porosity is (approximately) piecewise constant and decreasing, while pore velocity is likewise approximately piecewise constant, but increasing. As time increases the porosity develops to a (smooth) function that is monotone *increasing* within each layer, with sharp (negative) jumps between layers; while pore velocity is continuous and monotone decreasing in each layer, again with sharp (positive) jumps, in value, between layers.

The graphs of the particle concentration, $c(x,t)$, in Fig. 2a–e reveal that, for the chosen parameter values and porosity profiles, the multilayered membranes initially capture approximately 90% of particles in all cases, with

[1] We define the average porosity as $\phi_{i,\text{avg}}(t) = \int_0^1 \phi_i(x,t)\,\mathrm{d}x$.

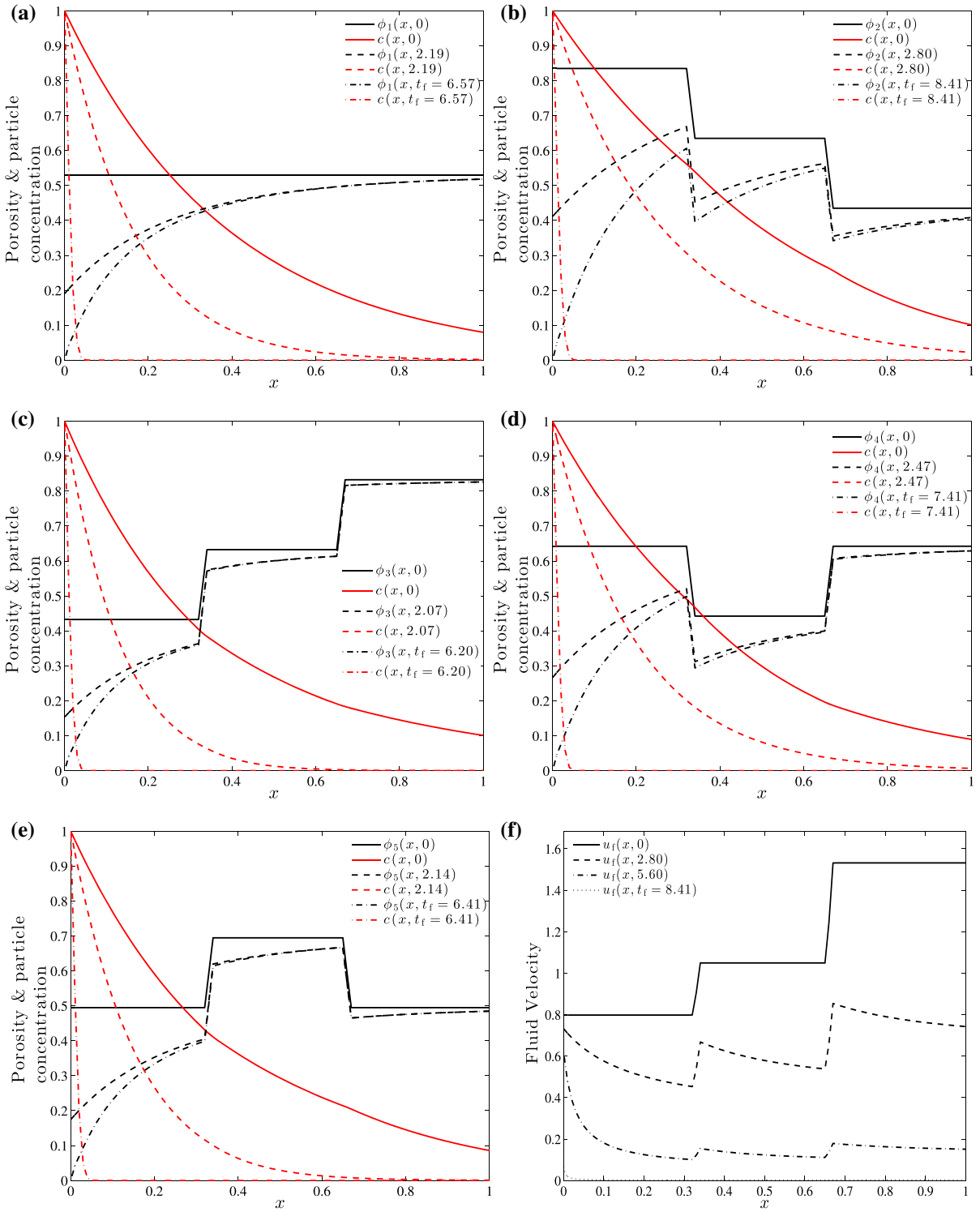

Fig. 2 Porosity profile and particle concentration as a function of dimensionless membrane depth at selected times up to final time (t_f, indicated in the legends) for different initial porosity profiles given in Eq. (27): **a** $\phi_1(x,0)$, **b** $\phi_2(x,0)$, **c** $\phi_3(x,0)$, **d** $\phi_4(x,0)$, **e** $\phi_5(x,0)$; **f** the cross-sectionally averaged fluid velocity u_f for initial porosity profile $\phi_2(x,0)$, with $\lambda = 1$, $\delta = 8$, and $r_0 = 1.5$

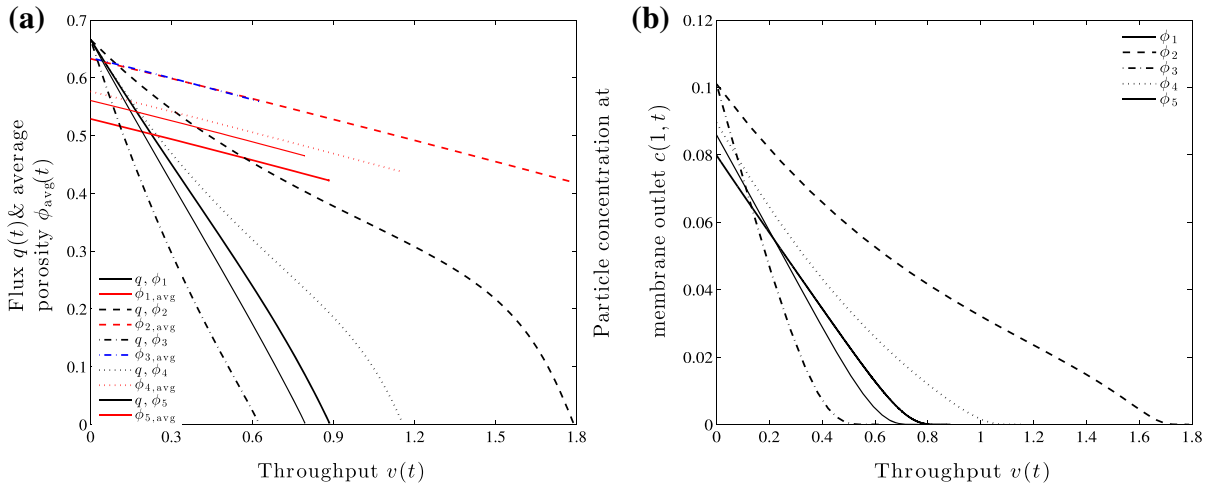

Fig. 3 **a** Total flux $q(t)$ and average porosity $\phi_{\text{avg}}(t)$; and **b** particle concentration at the downstream membrane, $c(1,t)$; versus throughput $v(t) = \int_0^t q(t')\mathrm{d}t'$, with $\lambda = 1$, $\delta = 8$, and $r_0 = 1.5$, for initial porosity profiles ϕ_1–ϕ_5 given in Eq. (27)

this proportion increasing to nearly 100% as time progresses.[2] Figure 2 also reveals that the filter with initial monotonically decreasing porosity profile, ϕ_2, has the desirable features that it captures particles more uniformly within the filter, and the clogging time (t_f, indicated in the figure legends) is about 28% longer than that for the filter with initially uniform porosity, ϕ_1.

A common experimental characterization of filter membrane performance is to plot the total instantaneous flux of filtrate through the membrane against the cumulative filtrate throughput at that time (see the definitions in Eq. (25)), which illustrates the membrane fouling behavior. Figure 3a shows the flux $q(t)$ and average porosity $\phi_{\text{avg}}(t)$ as a function of instantaneous throughput $v(t)$, for the five initial porosity profiles given in (27). The case in which the initial porosity profile decreases monotonically with depth (ϕ_2) gives significantly better performance (more total throughput or filtered fluid), while the membrane with initial porosity monotonically increasing along the filter depth (ϕ_3) gives the least total throughput, even though both filters have the same initial resistance ($r_0 = 1.5$) and the graphs of the average porosity $\phi_{\text{avg}}(t)$ for these two initial porosity profiles (ϕ_2 and ϕ_3) are indistinguishable (until the latter blocks completely). Another feature is that the flux-throughput curves in Fig. 3a are initially concave (at least for some scenarios), and become convex as total system blockage is approached. This change of curvature has been observed in other model simulations [10,12,14,41] as well as in experimental systems [40], and is typically attributed to a change in the dominant fouling mode, from adsorption to blocking.

In addition to total throughput, another important measure of filter membrane performance is particle removal (capture) efficiency, which addresses the proportion of particles the filter removes (captures) from the feed. Figure 3b shows the particle concentration at the downstream membrane surface, $c(1,t)$, as a function of instantaneous throughput, for each of the initial porosity profiles given in Eq. (27). In addition to confirming the results of Fig. 2, that all five membrane stacks simulated initially capture approximately 90% of particles in all cases, these graphs provide further information to distinguish between the particle capture performance of each membrane over its lifetime. The initially uniform porosity profile, ϕ_1 at first marginally outperforms (in terms of particle removal efficiency) all other cases considered here, but this does not persist at later times. The porosity profile that decreases monotonically with depth (ϕ_2), which performed best in terms of total throughput, exhibits the worst particle retention, over the entire time period simulated. These results are perhaps unsurprising when one considers that the membrane with the best (worst) initial particle removal efficiency is that with the lowest (highest) initial average porosity. However, an important performance indicator is the *initial* particle capture efficiency at $t = 0$, and the

[2] In many practical applications the desired particle retention by the membrane is much higher than this. These simulations are purely illustrative. The effect of model parameters on particle retention is investigated later.

fact that the differences in this criterion between all compared filters are relatively small is encouraging: so long as a membrane meets the target for initial particle removal, it should maintain or improve on this capture efficiency over its useful lifetime.

Figures 2 and 3 collectively confirm the conclusions of many previous studies (see e.g., [10,31–35] among others), that membranes with porosity decreasing in the direction of flow have longer life span and higher total throughput over the filter lifetime within industrially relevant parameter regimes. Additionally, among the equal-resistance filters considered here, as the initial average porosity of the membrane stack increases, the total filtrate throughput increases (Fig. 3a), but at the same time, the initial particle removal capability decreases (Fig. 3b). In other words, there is always a tradeoff between the particle removal capability and the total filtrate throughput. In the rest of this paper, we will focus on making these conclusions more precise by studying the effects of key model parameters on filter performance.

4.2 Effect of membrane properties

Different types of membrane (e.g.,, different membrane materials, different pore structure, etc.) exhibit different particle deposition properties. In the illustrative simulations thus far we fixed the values for the particle adsorption propensity coefficient λ, and the particle blocking coefficient δ. Since these parameters were chosen in the absence of firm experimental data, and will depend on the specific system under consideration, we now briefly investigate the effect of varying them to simulate different filtration regimes.

4.2.1 Effects of particle adsorption propensity

To examine the effect of adsorption propensity on the filtration efficiency, we first vary the dimensionless particle adsorption coefficient λ, which we suppose to change due to variation of the dimensional average adsorption rate of particles $\bar{\lambda}$ (see Table 2). We do this for the monotone decreasing initial porosity profile ϕ_2 given in Eq. (27), with $\delta = 8$ and initial resistance $r_0 = 1.5$ as previously.

In Fig. 4a, the porosity profile at final time t_f is plotted as a function of membrane depth, for four values of the particle deposition coefficient λ (but the same membrane structure in all cases). The corresponding flux-throughput curves and particle concentration in the filtrate versus throughput graphs are also shown in Fig. 4b and c, respectively. As the value of λ varies from small to large the model switches from blocking-dominated to adsorption-dominated, and there is a clear qualitative change in the shape of the flux-throughput performance curves from concave to convex (Fig. 4b).

Small values of λ may be interpreted as modeling the scenario where a substantial fraction of particles in the feed suspension are smaller than the pores in the more porous layer upstream, hence they are able to penetrate the upstream layer, but they may become trapped and adhere to the pore walls in the less porous layer downstream. Although this prolongs the lifetime of the filters (see values of t_f in Fig. 4a), the inferior particle retention makes small values of λ likely undesirable (see Fig. 4c). We note that membrane fouling can occur deep within the filter for sufficiently weak adsorption, as shown in Fig. 4a, $\lambda = 0.01$. In this case the adsorption is so weak that the complete blocking of the membrane occurs first in the membrane interior, an atypical situation and one that is undesirable from a practical viewpoint since the particle concentration at the membrane outlet is high in this case (see Fig. 4c). At the other extreme, large values of λ may be interpreted as modeling the scenario where particles tend to adhere to the membrane surface at a faster rate, which causes the membrane to foul quickly at the upstream side, while downstream portions remain minimally used. The price paid for this superior separation is, of course, a shorter lifetime due to the rapid fouling. In applications, a compromise must be made between achieving the desired separation with an acceptable filter lifetime.

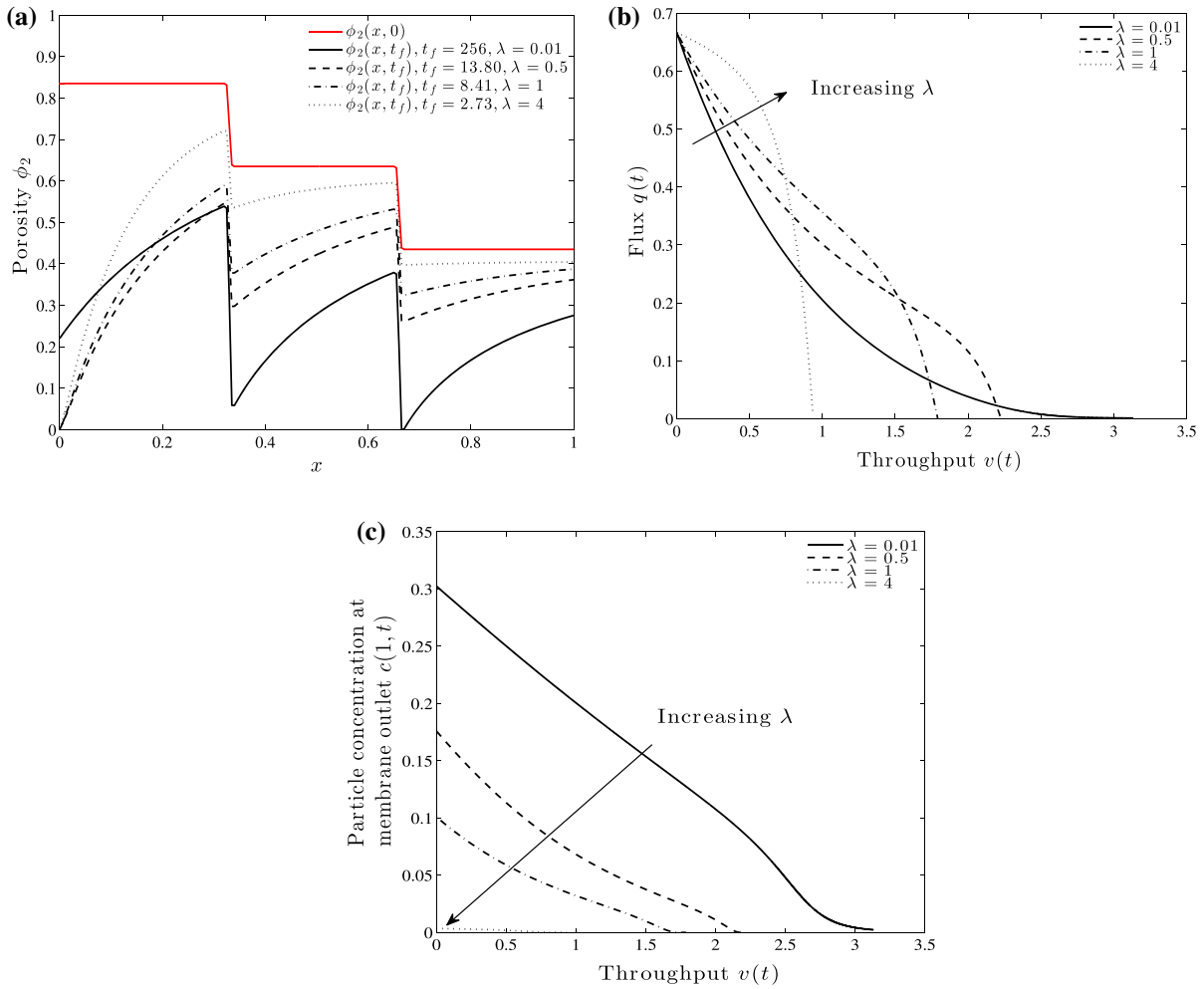

Fig. 4 Results for four different values of λ (corresponding to varying the dimensional average adsorption rate of particles $\bar{\lambda}$, see Table 2). **a** Black curves: Porosity profile $\phi_2(x, t_f)$ as a function of dimensionless membrane depth at final time t_f (indicated in the legend). Red curve is initial porosity $\phi_2(x, 0)$, see Eq. (27). **b** Total flux $q(t)$ and **c** particle concentration in filtrate $c(1, t)$, as functions of throughput $v(t) = \int_0^t q(t')\mathrm{d}t'$ for the same initial porosity profile (red curve in (**a**)), with $\delta = 8$ and $r_0 = 1.5$. (Color figure online)

4.2.2 Effects of pore blocking

We next briefly consider the effect of varying the blocking coefficient δ, here assumed to vary due to changes in the dimensional average blocking coefficient $\bar{\delta}$. We do this again for the monotone decreasing initial porosity profile ϕ_2 given in Eq. (27), with $\lambda = 1$ and dimensionless initial filter resistance $r_0 = 1.5$. Figure 5 shows the results: Fig. 5a plots the porosity profile within the filter at the final time t_f as a function of membrane depth; while Fig. 5b and c shows flux and particle concentration in the filtrate as functions of throughput, each for several values of δ (but the same membrane structure in all cases). Recall that $\bar{\delta}$ was used in the timescale in (12): here, rather than consider a different timescale for each δ-value illustrated, we use the same value $\delta = h\bar{\delta} = 8$ in (12) to nondimensionalize the time in all cases illustrated, so that results may be directly compared. As δ increases, the dominant mode of fouling changes from adsorption-dominated to blocking-dominated (compare Figs. 5b and 4b).

We may interpret small values of δ as modeling the physical case in which the ratio of typical particle size to typical pore size is small, hence adsorption is the dominant fouling mechanism (at least in the more porous upstream layer, the fouling of which dominates overall system behavior). For large δ particles are likely to be larger than pores

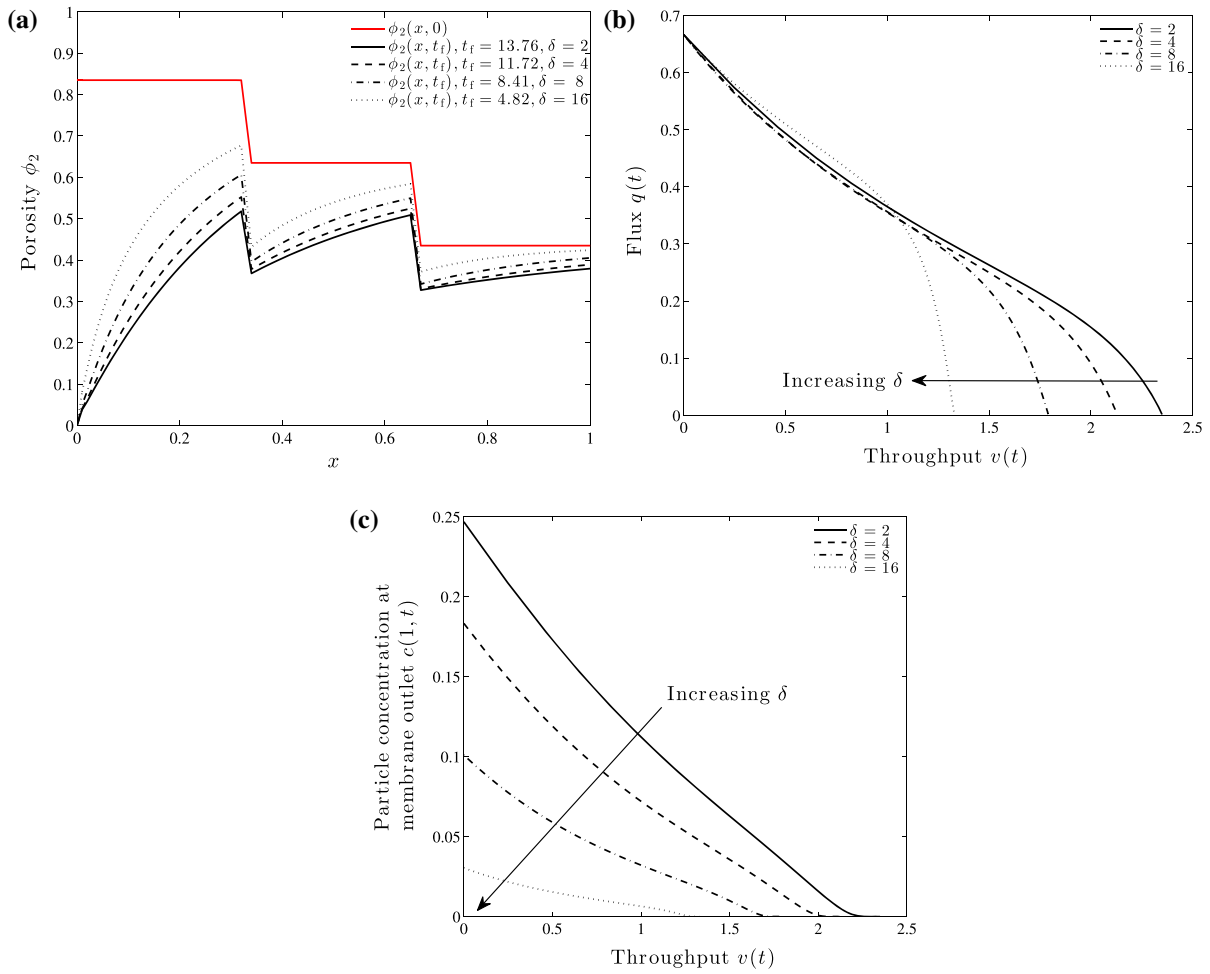

Fig. 5 Results for four different values of the blocking coefficient δ. **a** Black curves: Porosity profile $\phi_2(x, t_f)$ as a function of dimensionless depth at final time t_f (indicated in the legend). Red curve: Initial porosity profile $\phi_2(x, 0)$, see Eq. (27). **b** Flux $q(t)$ and **c** particle concentration in the filtrate, $c(1, t)$, as functions of throughput $v(t) = \int_0^t q(t')dt'$, for the same initial porosity profile $\phi_2(x, 0)$, with $\lambda = 1$ and $r_0 = 1.5$

in the upstream layer, so blocking dominates over adsorption. Since the adsorptive fouling coefficient λ remains fixed for all simulations in Fig. 5, the rate of overall fouling increases with δ. Total system resistance then increases more rapidly, which leads to decreased filter lifetime as δ increases (see values of t_f in Fig. 5a). Fig. 5b and c exemplifies the tradeoffs inherent in filtration: larger values of δ give less total throughput over the filter lifetime, but better separation.

4.2.3 Effects of membrane thickness

It is also of interest to understand the influence of membrane thickness h, which appears in both dimensionless parameters discussed above: $\lambda = (h^2\bar{\lambda}\mu)/(p_0\chi)$ and $\delta = h\bar{\delta}$ (see Table 2). To examine the effect of h on filtration we must therefore vary both λ and δ, with $\delta \propto \sqrt{\lambda}$. Note that changing membrane thickness necessarily changes the resistance (unless drastic changes are made to other quantities): a thinner membrane has a lower resistance, and a thicker membrane provides a higher resistance. Therefore, in this subsection, we are no longer considering equal initial resistance membranes, but only membranes with equal initial average porosity. Figure 6 shows the results, plotting flux and particle concentration in the filtrate as functions of throughput, for several different membrane

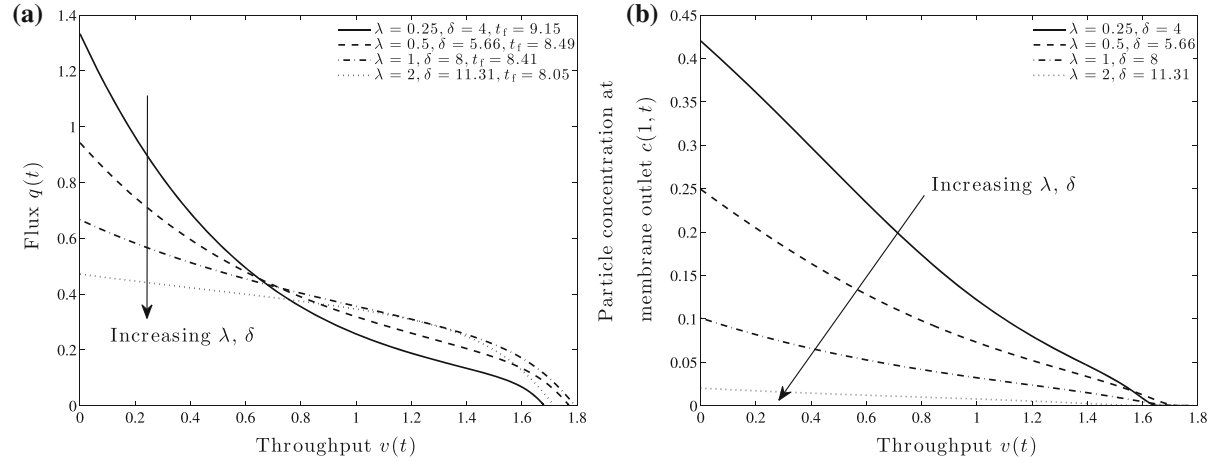

Fig. 6 **a** Flux $q(t)$ and **b** particle concentration in filtrate, $c(1,t)$, as functions of throughput $v(t) = \int_0^t q(t')\mathrm{d}t'$, for the initial porosity profile $\phi_2(x,0)$ given in Eq. (27), with initial average porosity $\phi_{2,\text{avg}} = 0.6350$, for four different values of $\lambda \propto \delta^2$ (corresponding to varying membrane thickness h). See text for more details

thicknesses h. Observe that h appears in both the time scale and the velocity scale as given in Eq. (12); in order to compare results directly, the fixed value of h corresponding to $\lambda = 1, \delta = 8$ is used for these scales in all cases illustrated here.

For small values of λ, δ (corresponding to thin membranes), the feed suspension transits the membrane too quickly, resulting in poor particle retention, with a significant fraction of particles remaining suspended in the filtrate. This results in slow fouling, which prolongs the life span of the filter; but the poor separation makes this filter design undesirable. For large values of λ, δ (corresponding to thick membranes), the feed suspension remains within the membrane long enough to deposit nearly all of the carried particles, but the superior particle removal performance is offset by rapid fouling. Interestingly, changing the membrane thickness appears to have a much smaller impact on the overall performance (more total throughput and longer life span) than does changing the membrane particle adsorption and blocking coefficients, suggesting that membrane material properties play a more important role in the overall performance.

4.3 n-Layer membranes

The results of Sect. 4.2 above provide some insight into how simple membrane stacks with different porosity layers behave as filters, and the effects of key model parameters. We now generalize our investigation to consider the filtration performance of a membrane composed of a stack of n layers of thicknesses d_i, $i = 1, 2, \ldots, n$, where each layer has constant initial porosity. As in the preceding 3-layer sample simulations, to avoid numerical issues we simulate only continuous porosity profiles, which vary rapidly across a layer interface, by using an initial porosity profile of the form

$$\phi(x,0) = \phi_{\text{avg}} + \frac{1}{2}\sum_{i=1}^{n-1} b \tanh(400(x - x_i)), \tag{28}$$

where ϕ_{avg} is the initial average porosity of the membrane, b is the (fixed) difference between the initial porosity of two successive layers, $x_i = \sum_{j=1}^{i} d_j$, $i = 1, 2, \ldots, n-1$, are the locations of the interfaces between two successive layers, and the factor of 400 was chosen to give sufficiently rapid variations in porosity across layer

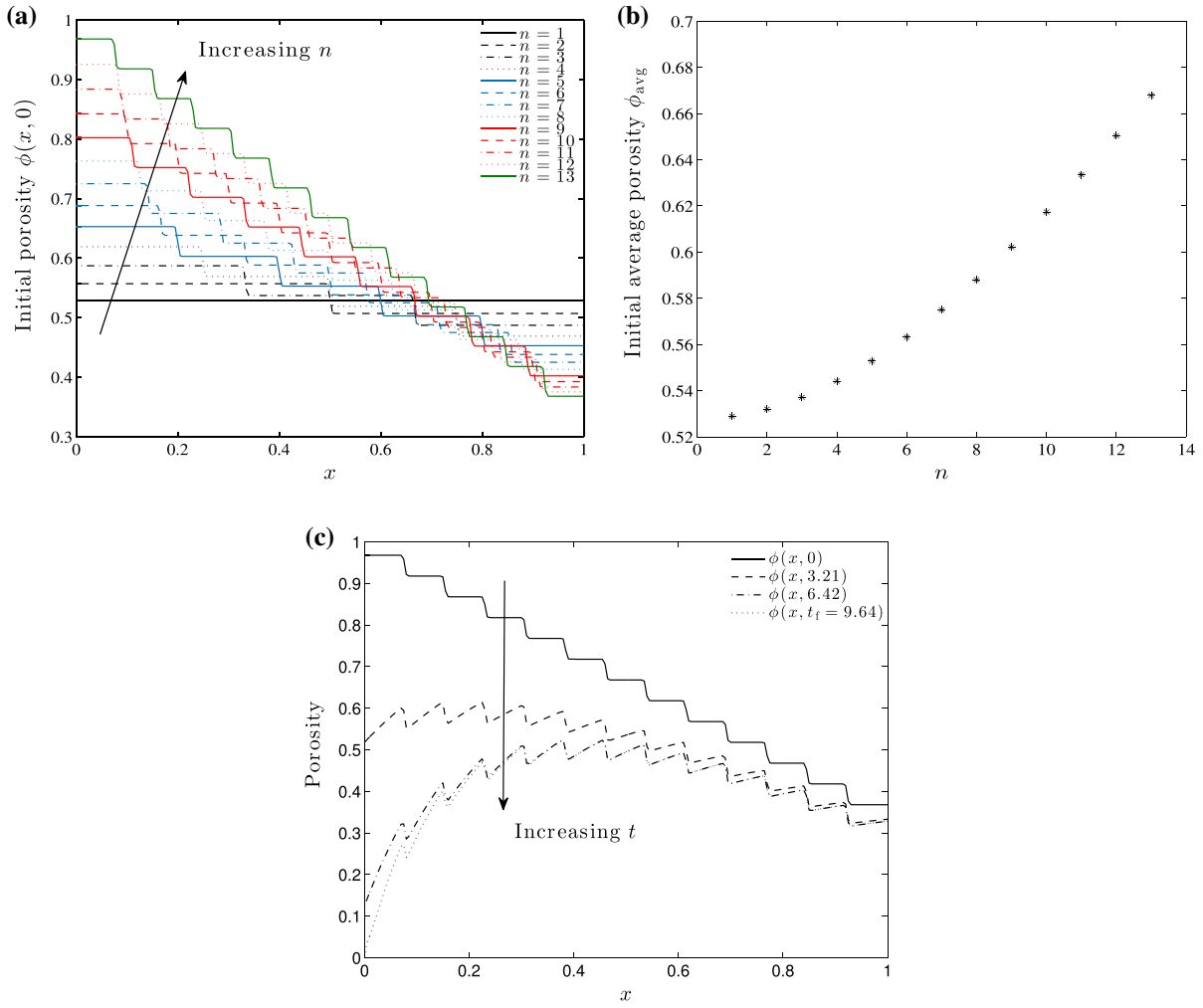

Fig. 7 **a** Initial porosity profile given in (28) as a function of dimensionless membrane depth, for thirteen values of n. **b** Initial average porosity as a function of number of layers. **c** Evolution of porosity profile of Eq. (28) as a function of dimensionless membrane depth, with $n = 13$. Other parameter values are $b = -0.05$, $\lambda = 1$, $\delta = 8$, and $r_0 = 1.5$

junctions. For a given initial membrane resistance r_0 and a fixed value of b, the initial average porosity of the membrane ϕ_{avg} is then determined by using (26).

We first consider the case where all layers have equal thickness, $d_i = 1/n, i = 1, \ldots, n$. Figures 7 and 8 illustrate the effect of changing the number of layers n in the filter stack. In Fig. 7a, we plot the initial porosity profiles of (28), for $n = 1, \ldots, 13$, with $b = -0.05$, while Fig. 7b shows the initial average porosity ϕ_{avg} as a function of n. Note that in all cases, the initial average membrane resistance is the same: $r_0 = 1.5$, while the initial average porosity, ϕ_{avg} increases with increasing n, taking values in the range (0.5289,0.6679). Figure 7c shows the evolving porosity profile $\phi(x, t)$ within the feed as it passes through the membrane, for $n = 13$ and $b = -0.05$. As time increases, the porosity decreases most rapidly near the membrane inlet and develops to a (smooth) function that is monotone increasing within each layer, with sharp (negative) jumps between layers, as seen earlier in Fig. 2b. For brevity of presentation, the results for the other twelve initial porosity profiles considered (which show qualitatively similar features) are not shown here.

Figure 8 summarizes the key results and predictions for different numbers of layers. In Fig. 8a, we plot flux as a function of throughput for the same family of initial porosity profiles, again with $n = 1, \ldots, 13$, and particle

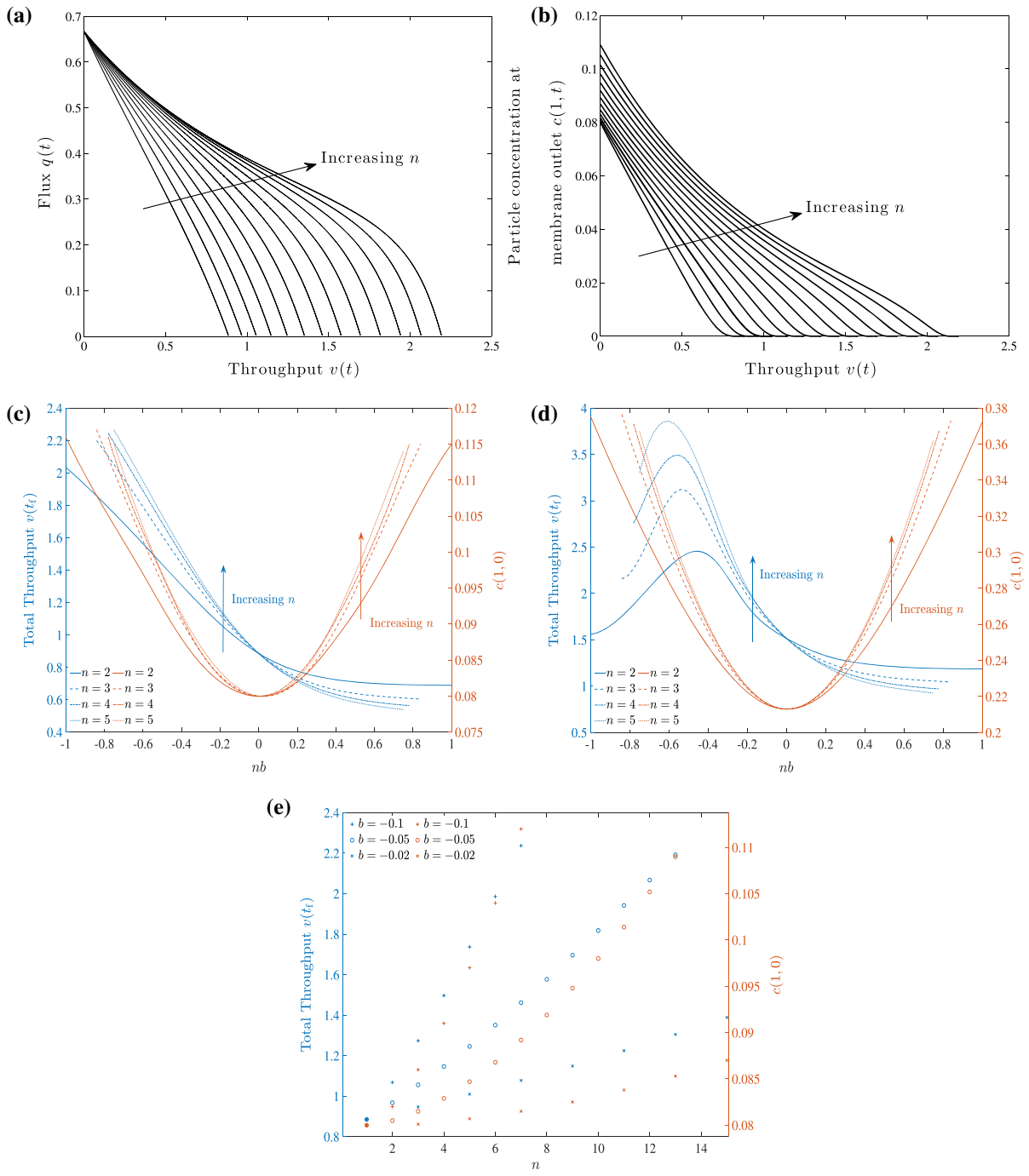

Fig. 8 **a** Flux and **b** particle concentration in filtrate $c(1,t)$ as functions of throughput for initial porosity profile given in Eq. (28), with porosity difference between two consecutive layers $b=-0.05$ and $\lambda=1$, for thirteen values of $n=1,2,\ldots,13$. **c** and **d** Total throughput $v(t_f)$ and initial particle concentration in filtrate $c(1,0)$ as a function of porosity gradient nb for initial porosity profile given in Eq. (28), for four different values of $n=2,3,4,5$, with different values of λ: **c** $\lambda=1$ and **d** $\lambda=0.01$. **e** Total throughput $v(t_f)$ and initial particle concentration in filtrate $c(1,0)$ as a function of number of layers for initial porosity profile given in Eq. (28), with $\lambda=1$, for three different scenarios. Other parameter values are $\delta=8$ and $r_0=1.5$

deposition coefficient $\lambda = 1$. Increasing the number of layers n while fixing the porosity difference between two consecutive layers b to be a negative (positive) constant leads to an increase (decrease) in the final total throughput (the results for positive b, known to be undesirable in practical applications, are not shown). Figure 8b shows the corresponding particle concentrations in the filtrate, $c(1, t)$, as a function of throughput, for fixed negative b. Although (as just observed) the total throughput increases with the number of layers n, there is a simultaneous decrease in particle retention capability of the membrane, evidenced by an increase in the particle concentration in the filtrate. We hypothesize that this loss of retention capability is because, as the number of (thinner) individual layers is increased at fixed resistance, there is a corresponding increase in the initial average porosity of the entire membrane (seen in Fig. 7b), which in turn leads to a slight decrease in removal efficiency. As long as the retention capability of the membrane is acceptable, however, this decrease in retention capability may be compensated by the increase in final total throughput, which can be significant. This trend of increasing layer number being associated with diminished particle retention but increased throughput was found numerically to hold for any combinations of $\lambda \in (0.25, 4)$ and $\delta \in (2, 16)$.

Figure 8c shows total throughput $v(t_f)$ and initial particle concentration in the filtrate as a function of nb (nb can be interpreted as a global porosity gradient, since the porosity changes by an amount b over a lengthscale $1/n$), for four values of n and $\lambda = 1$. In all cases $v(t_f)$ is monotone decreasing with nb, with the rate of decrease faster for larger n. As already observed (Fig. 8b), $c(1, 0)$ increases moderately as n increases, but we now also see a strong dependence on nb. In particular, the filters with either decreasing or increasing porosity in the membrane depth are less desirable than those of uniform porosity as regard initial particle removal (though not as regard total throughput). As expected, all layer numbers give the same result when $nb = 0$ and the layers all have the same porosity. These results bear out our previous conclusions, that within industrially relevant parameter regimes, larger (negative) porosity gradients within a filter membrane are favorable for increasing throughput and filter lifetime but at the expense of moderately poorer initial particle retention: generally speaking, the largest (negative) porosity gradient commensurate with acceptable particle removal should be used for maximal useful filter lifetime. If, however, we set aside concerns about acceptable particle removal and choose a very small value for the deposition coefficient λ, then it is possible to obtain an optimal (negative) membrane porosity gradient leading to membrane pore closure at an internal point, as seen in [10,15], for example. Figure 8d shows results analogous to Fig. 8c but for $\lambda = 0.01$, with total throughput plotted as a function of porosity gradient, nb, for four different values of n. The results demonstrate that for sufficiently small λ, the optimal arrangement for maximizing throughput is to have the porosity gradually decreasing with depth and increase the number of filter layers, as also reported in [15]. The obvious downside is that particle concentration at the membrane outlet is unacceptably high. We emphasize again that all results plotted in Fig. 8 are for membranes of equal initial resistance.

Figure 8e gives an alternative representation of the results for $\lambda = 1$, with total throughput $v(t_f)$ and initial particle concentration in the filtrate $c(1, 0)$ plotted as a function of number of layers n, for three negative values of b: in all cases $v(t_f)$ and $c(1, 0)$ increase with n. Increasing $|b|$ results in a steeper increase in total throughput with n, indicating a longer time to complete fouling of the membrane, but as usual, the tradeoff is decreased particle removal efficiency (higher particle concentration in the filtrate). Overall, we can see that, provided the desired particle removal efficiency can be satisfied, increasing the size of porosity jumps between layers (larger $|b|$), and increasing the number of layers n, both lead to the desirable outcome of increased total throughput and filter lifetime.

We conclude with a brief discussion of whether it may be advantageous to allow layers of different thicknesses (all simulations so far have been for layers of equal thickness). To avoid introducing a large number of additional parameters, we restrict attention to the case where the thickness of adjacent layers follows a geometric progression, with $d_i = \gamma^{i-1} d_1$ for $i = 2, 3, \ldots, n$, and therefore the locations of the interfaces between successive layers are $x_i = d_1 \sum_{j=1}^{i} \gamma^{j-1}$, with $d_1 = (1 - \gamma)/(1 - \gamma^n)$. Note that $\gamma = 1$ corresponds to equal-thickness layers as studied previously (with $d_1 \to 1/n$), while if $\gamma > 1$ ($\gamma < 1$) layer thickness increases (decreases) in the depth of the membrane. We again assume a fixed change in initial porosity, b, between adjacent layers, and as before, only equal-resistance (at $t = 0$) membranes are compared.

Figure 9 shows total throughput $v(t_f)$ and initial particle concentration in filtrate $c(1, 0)$ as functions of γ, for several different scenarios (two values of n and three values of b). For $b > 0$ (initial porosity increases with depth,

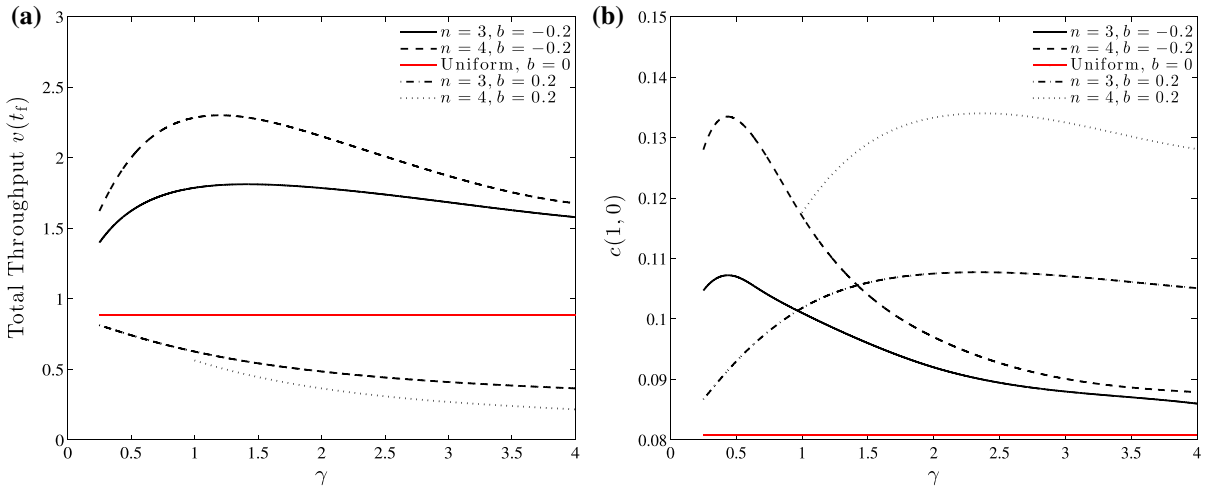

Fig. 9 **a** Total throughput $v(t_f)$ and **b** initial particle concentration in filtrate $c(1, 0)$ as a function of γ for initial porosity profiles as in Eq. (28), for five different scenarios as noted in the legend, with $\lambda = 1$, $\delta = 8$. In all cases the initial membrane resistance is $r_0 = 1.5$

a scenario not normally considered in applications) we see that the total throughput decreases monotonically with γ in the two cases considered. Presumably this is because as γ increases, the low-porosity upstream layers are becoming thinner relative to the high-porosity downstream layers. In order to maintain the fixed initial resistance, however, the initial porosity of the thinnest upstream layers must decrease (compared to smaller-γ scenarios) which, since these layers foul first, means rapid fouling and closure of these layers, and filter failure. We note that the total throughputs for all $b > 0$ cases considered here are less than the total throughput for the initially uniform porosity case $b = 0$ (red line in Fig. 9), again confirming that membranes with initially increasing porosity profiles have reduced life span and decreased efficiency as measured by this total throughput metric.

For $b < 0$ (initial porosity decreases with depth), the curves of total throughput versus γ exhibit a well-defined maximum: we find that the maximal total throughput is achieved when γ is slightly larger than 1, corresponding to a scenario in which each succeeding layer is slightly thicker than the preceding layer. Similar results have been noted previously [11]. Nonetheless, this result is rather surprising given our previous simulation results showing the rapid membrane fouling that occurs at the upstream surface. One might expect that the maximal total throughput would be achieved when $\gamma < 1$, corresponding to a thicker high-porosity layer at the upstream, which would help delay membrane fouling and total pore closure in this region for a longer period of time. We hypothesize that the presence of the maximum could be explained as follows: with $b < 0$ and a fixed initial resistance, increasing γ through small values (*i.e.,* changing from a system where upstream layers are considerably thicker than downstream layers to one where the thickness differences between adjacent layers are less severe) while maintaining fixed resistance results in increased initial porosity of upstream layers, which at first delays fouling and increases total throughput, as also seen earlier in Fig. 3a. However, as we continue to increase γ the upstream layers necessarily become thinner; thinner than the downstream layers when $\gamma > 1$, and at some point, when the top layers become very thin and very porous, particles are able to penetrate into more of the downstream layers, which are less porous and clog faster. Therefore, total throughput will eventually decrease once γ increases beyond a certain value.

5 Discussion and conclusions

We have presented a simple mathematical model to describe the key elements of separation and fouling in a multilayered membrane filter, which includes Darcy flow through the multilayered membrane, advection-dominated transport and deposition of particles within the porous membrane stack, and variations in porosity due to fouling (particle deposition). Our model accounts for two distinct mechanisms of fouling: adsorption of small particles

within pores, and pore blockage associated with deposition of large particles. Assuming that the timescale for flow to transit the membrane is much shorter than that associated with fouling-induced changes to porosity, the resulting system is quasi-static, with time dependence appearing only in the porosity evolution equation.

Given the complexity of the membrane structure and the chemical interactions between the filtrate particles and the membrane material, which vary from one application to another, our simplified model necessarily contains several parameters that may be difficult to measure for a given membrane-filtrate system, and that will vary from one system to another. In the absence of detailed experimental data, values for many of these parameters are unavailable, hence in order to carry out simulations of our model, we have chosen parameter values (summarized in Table 2) based on what is known to occur (qualitatively) in real membrane-filtrate systems.

Key challenges facing membrane scientists and engineers are how to maximize the total throughput while simultaneously ensuring adequate particle removal efficiency (requirements that are necessarily in conflict); and how to achieve more uniform adsorption in the membrane, which would presumably prolong the life of the filter. Since porosity gradients are known to influence filter performance significantly, our study focused on how porosity gradients affect the fouling and performance of multilayer membrane filters. Our results confirm the conclusions of previous studies [10,30–35] that using membranes whose initial porosity decreases with depth can prolong the life span and increase the total throughput of filtrate over the filter lifetime.

To illustrate the differences in the two fouling mechanisms considered, we briefly investigated the effects of changing the model parameters λ (dimensionless particle/membrane adsorption coefficient) and δ (dimensionless pore-blocking coefficient) in Sect. 4.2, focusing on the most relevant case in which the initial porosity of the multilayered membrane decreases with depth. Only equal-resistance membranes were compared in the study of these two parameters.

We observe (Sect. 4.2.1) that small values of the adsorption coefficient λ yield greater total throughput and a longer filter life span. However, if λ is too small then the particle retention capability of the membrane may be too low. As λ varies from small to large there is a qualitative change in the shape of the flux-throughput performance curves, as the model switches from blocking-dominated to adsorption-dominated. We also find (Sect. 4.2.2) that if the dimensionless blocking coefficient δ is small (pore blocking less important), the total throughput and clogging time increase. Again, however, this increased throughput and membrane lifetime are achieved at the expense of decreased particle removal capability. As δ increases, the dominant mode of fouling changes from adsorption-dominated to blocking-dominated.

While the parameters λ and δ are strongly dependent on the feed solution (specifically, the particles it contains), which are not under the manufacturer's direct control, certain design parameters such as the membrane thickness h, the total number of layers n, the relative thickness of those layers, and how porosity varies between adjacent layers in the stack are easily modified in the manufacture process. We therefore investigated these features also, to see what can be deduced about how to structure a layered membrane for optimal filtration performance (maximizing throughput of filtered fluid and filter lifetime, while removing an acceptable fraction of particles).

The role of total membrane thickness h is studied in Sect. 4.2.3. Here, membranes with three equal-thickness layers are compared. In all cases the initial porosities of corresponding layers in the stack are the same; only the thickness of the layers varies. Hence, varying the total membrane thickness h necessarily leads to systems with different net resistances (elsewhere only equal-resistance membranes were compared). We observe that thin membranes foul slowly, while thick membranes foul rapidly. If the membrane is too thin, filtration may be too fast to give good particle retention. On the other hand, thick membranes give better separation because the feed remains within the membrane for longer. The desired level of particle separation from the feed solution varies from one application to another, hence the best choice for overall membrane thickness will depend on the application.

In Sect. 4.3, we extended our study to membranes with a larger number of layers, of equal and unequal thicknesses, to investigate the sensitivity of membrane fouling to these factors. We found that increasing the number of layers can significantly increase total throughput and delay membrane failure time for membranes whose initial porosity decreases with depth, but the tradeoff is with a moderately poorer initial particle retention (see Fig. 8e). We also found that increasing the (initial) porosity gradient results in a significantly increased throughput for membranes with porosity decreasing in depth, but again the tradeoff is a corresponding decrease in initial particle retention (see

Fig. 8c), which may or may not be acceptable to the end user. If we ignore such concerns then for very low values of the deposition coefficient λ one can obtain an optimal (negative) membrane porosity gradient that leads to membrane pore closure at an internal point. Figure 8d demonstrates that for a very low value of deposition coefficient, $\lambda = 0.01$, the optimal arrangement for maximizing throughput is to have porosity gradually decreasing with depth, and a large number of filter layers. Additionally, we found that the optimal layer thickness distribution that maximizes total throughput corresponds to a membrane stack in which layer thickness increases slightly between successive layers in the depth of the membrane (see Fig. 9). Although creating multilayered membrane filters with a large number of layers of nonequal thickness could be manufacturally challenging, it appears to offer advantages both in terms of maximizing total throughput and filter life span.

Finally, we remind the reader that our results were obtained using parameters that we believe to be plausible, but that were not measured directly from a detailed experimental dataset. Given reliable estimates of our model parameters for any given filtration system, our model offers excellent potential for predicting the optimal layered filter configuration.

Acknowledgements The work carried out in this paper arose from a problem presented at the 2017 Mathematical Problems in Industry workshop, held at New Jersey Institute of Technology. L.J.C. and P.S. acknowledge financial support from the National Science Foundation (NSF) under Grants No. DMS-1261596 and No. DMS-1615719. P.S. was also supported in part by the NSF Research Training Group in Modeling and Simulation Grant No. RTG/DMS-1646339 as well as a travel award and an Institutional Support of Research and Creativity (ISRC) grant provided by New York Institute of Technology.

Declarations

Conflict of interest The authors declare that they have no conflict of interest.

Appendix A: Constant flux case

Membrane fouling is often characterized in laboratory experiments by challenging the membrane with a constant pressure drop. However, many industrial micro-filtration applications operate at constant flux, and there are few papers that compare these modes of operation for multilayered membranes [42]. In this appendix, we briefly outline how the results change if boundary conditions of constant flux are imposed. We first outline the modifications to the model in Sect. 3, then present sample numerical simulations.

A.1 The model for specified flux

The original model (1)–(11) remains unchanged except that the boundary condition for the pressure at the upstream membrane surface is now time-dependent, $p_0(t)$ (the membrane resistance increases in course of time, therefore the imposed pressure at the membrane upstream should increase to sustain the flux). We nondimensionalize the model using the same scalings as in (12), except for

$$p = \frac{h\mu}{u_0 \chi} p^*, \quad (u, u_\mathrm{f}) = u_0 (1, u_\mathrm{f}^*). \tag{29}$$

The dimensionless model is reduced to

$$c = \exp\left[- \int_0^x \tilde{\lambda}\phi^{2/3} + \tilde{\delta}(1 - \phi^{1/3}) \, \mathrm{d}x' \right], \tag{30}$$

$$\frac{\partial \phi}{\partial t} = -\frac{\tilde{\lambda}}{\tilde{\delta}} \phi^{2/3} c - (1 - \phi^{1/3}) c, \tag{31}$$

where $\tilde{\lambda} = (h\bar{\lambda})/u_0$, $\tilde{\delta} = h\bar{\delta}$, $\tilde{\lambda}/\tilde{\delta} = \bar{\lambda}/u_0\bar{\delta}$, the initial condition is as in (24), and the modified Darcy pressure p within the membrane is given by

$$p = \int_x^1 \frac{(1-\phi)^2}{\phi^3}\, \mathrm{d}x'. \tag{32}$$

Note that the pressure at the upstream membrane surface $p(0, t)$ can be calculated by setting $x = 0$ in (32).

A.2 Results

Figure 10a–e shows results for the same initial porosity profiles given in (27). Figure 10f shows the inverse pressure drop as a function of throughput for each of those porosity profiles. We observe that there is a significant difference in fouling behavior between the two operating modes. In contrast to the constant pressure simulations, the rate of fouling near the membrane inlet is observed to be less severe, which enables fouling to occur much more uniformly within the multilayered membrane. This is particularly true of membranes whose initial porosity profile is monotonically decreasing with depth, illustrated here by ϕ_2. As the resistance increases with time due to fouling, the pressure drop must be increased to maintain constant flux. Thus we plot the inverse pressure drop instead of flux as a function of throughput in Fig. 10f to illustrate the fouling behavior, for the five initial porosity profiles given in Eq. (27). If the fluid is maintained at constant flux until total blockage is reached, the pressure must increase to infinity, which is of course not practical. In most industrial filtration systems, the fluid is pumped at constant flux (flow rate) till the maximum pressure (based on practical constraints of the system under consideration) is reached and then the fluid handling system is automatically switched to the constant pressure operating mode, with the pressure fixed at this maximal value (this can then be described by the model as discussed in Sect. 3). As with the constant pressure simulations, the case in which the initial porosity profile decreases monotonically with depth (ϕ_2) gives significantly better performance (more total throughput and the longest time until total blockage is reached), while the membrane with initial porosity profile monotonically increasing along the filter depth (ϕ_3) gives the least total throughput and the shortest life span.

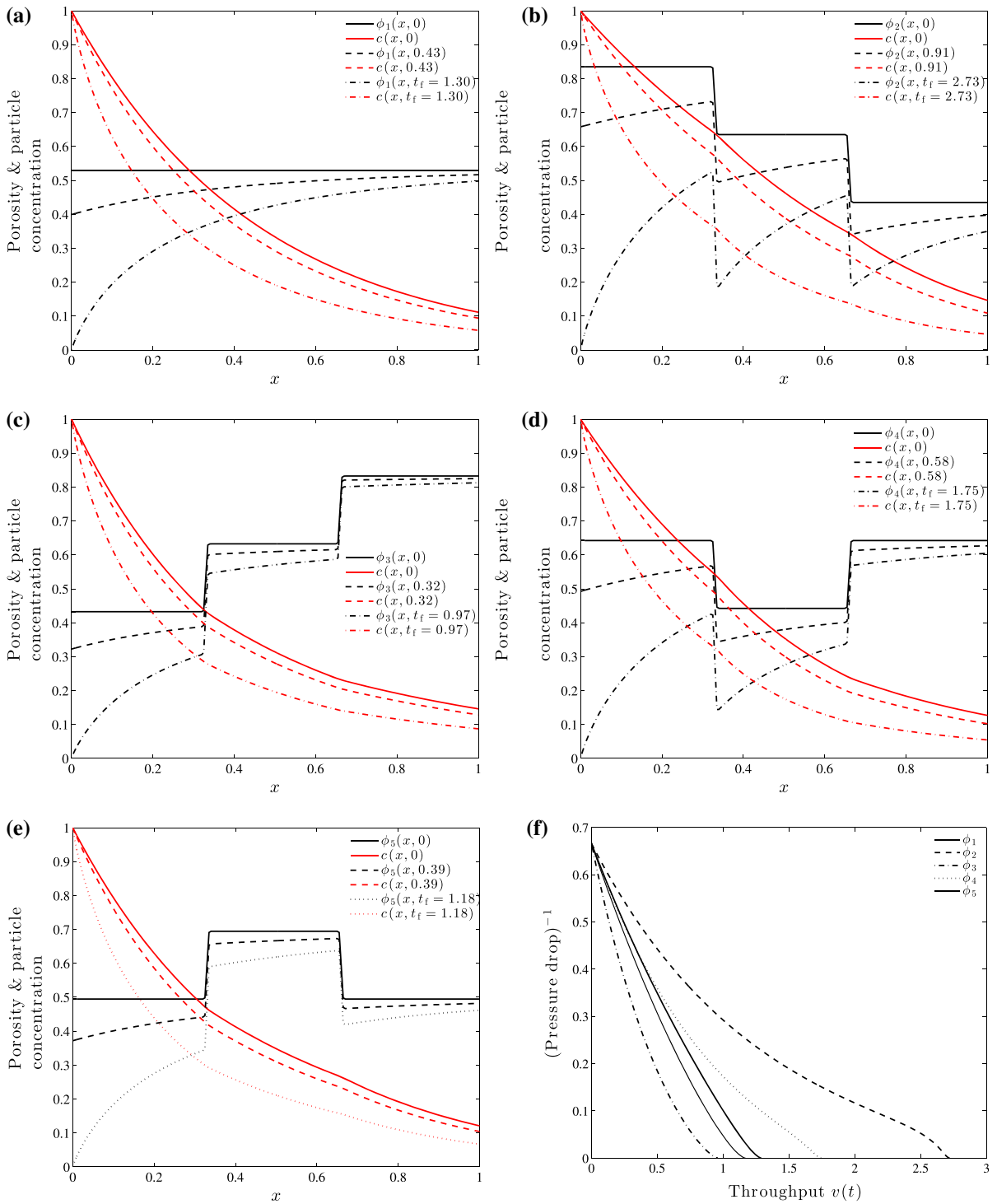

Fig. 10 Simulations at constant flux: porosity profile and particle concentration as functions of dimensionless space at selected times up to final time (t_f, indicated in the legends) for different initial porosity profiles given in Eq. (27): **a** $\phi_1(x,0)$, **b** $\phi_2(x,0)$, **c** $\phi_3(x,0)$, **d** $\phi_4(x,0)$, **e** $\phi_5(x,0)$, and **f** inverse pressure drop as a function of throughput for these initial porosity profile, with $\tilde{\lambda}=1$, $\tilde{\delta}=8$, and $r_0=1.5$

References

1. Iritani E (2013) A review on modeling of pore-blocking behaviors of membranes during pressurized membrane filtration. Dry Technol 31:146–162
2. Bolton G, LaCasse D, Kuriyel R (2006) Combined models of membrane fouling: development and application to microfiltration and ultrafiltration of biological fluids. J Membr Sci 277:75–84
3. Bolton GR, Boesch AW, Lazzara MJ (2006) The effects of flow rate on membrane capacity: development and application of adsorptive membrane fouling models. J Membr Sci 279:625–634
4. Ho C-C, Zydney AL (1999) Effect of membrane morphology on the initial rate of protein fouling during microfiltration. J Membr Sci 155:261–275
5. Ho C-C, Zydney AL (2000) A combined pore blockage and cake filtration model for protein fouling during microfiltration. J Colloid Interface Sci 232:389–399
6. Daniel RC, Billing JM, Russell RL, Shimskey RW, Smith HD, Peterson RA (2011) Integrated pore blockage-cake filtration model for crossflow filtration. Chem Eng Res Des 89:1094–1103
7. Van der Sman R, Vollebregt H, Mepschen A, Noordman T (2012) Review of hypotheses for fouling during beer clarification using membranes. J Membr Sci 396:22–31
8. Sanaei P, Richardson G, Witelski T, Cummings L (2016) Flow and fouling in a pleated membrane filter. J Fluid Mech 795:36–59
9. Sun Y, Sanaei P, Kondic L, Cummings LJ (2020) Modeling and design optimization for pleated membrane filters. Phys Rev Fluids 5:044306
10. Sanaei P, Cummings LJ (2017) Flow and fouling in membrane filters: effects of membrane morphology. J Fluid Mech 818:744–771
11. Sanaei P, Cummings LJ (2018) Membrane filtration with complex branching pore morphology. Phys Rev Fluids 3:094305
12. Sanaei P, Cummings LJ (2019) Membrane filtration with multiple fouling mechanisms. Phys Rev Fluids 4:124301
13. Gu B, Renaud D, Sanaei P, Kondic L, Cummings L (2020) On the influence of pore connectivity on performance of membrane filters. J Fluid Mech 902
14. Liu SY, Chen Z, Sanaei P (2020) Effects of particles diffusion on membrane filters performance. Fluids 5:121
15. Griffiths I, Kumar A, Stewart P (2016) Designing asymmetric multilayered membrane filters with improved performance. J Membr Sci 511:108–118
16. Van Rijn CJM (1998) Membrane filter and a method of manufacturing the same as well as a membrane. US Patent 5,753,014
17. Wollinsky KH, Saefkow MW (1995) Filter for liquor filtration. US Patent 5,462,667
18. Koch E (1984) Multi-layer filter. US Patent 4,483,771
19. Yoon K, Kim K, Wang X, Fang D, Hsiao BS, Chu B (2006) High flux ultrafiltration membranes based on electrospun nanofibrous PAN scaffolds and chitosan coating. Polymer 47:2434–2441
20. Peters JE (1988) Multilayer membrane separator. US Patent 4,735,718
21. Wang N, Si Y, Wang N, Sun G, El-Newehy M, Al-Deyab SS, Ding B (2014) Multilevel structured polyacrylonitrile/silica nanofibrous membranes for high-performance air filtration. Sep Purif Technol 126:44–51
22. Chang C-L, Chang M-S (2004) Preparation of multi-layer silicone/PVDF composite membranes for pervaporation of ethanol aqueous solutions. J Membr Sci 238:117–122
23. Fatt I et al (1956) The network model of porous media. Trans AIME 207:144–181
24. Rege S, Fogler HS (1987) Network model for straining dominated particle entrapment in porous media. Chem Eng Sci 42:1553–1564
25. Ioannidis MA, Chatzis I (1993) Network modelling of pore structure and transport properties of porous media. Chem Eng Sci 48:951–972
26. Duclos-Orsello C, Li W, Ho C-C (2006) A three mechanism model to describe fouling of microfiltration membranes. J Membr Sci 280:856–866
27. Fernández XR, Rosenthal I, Anlauf H, Nirschl H (2011) Experimental and analytical modeling of the filtration mechanisms of a paper stack candle filter. Chem Eng Res Des 89:2776–2784
28. Li W-W, Sheng G-P, Wang Y-K, Liu X-W, Xu J, Yu H-Q (2011) Filtration behaviors and biocake formation mechanism of mesh filters used in membrane bioreactors. Sep Purif Technol 81:472–479
29. Nakamura K, Orime T, Matsumoto K (2012) Response of zeta potential to cake formation and pore blocking during the microfiltration of latex particles. J Membr Sci 401:274–281
30. Burggraaf A, Keizer K (1991) Synthesis of inorganic membranes. Inorganic membranes synthesis, characteristics and applications. Springer, New York
31. Barg S, Koch D, Grathwohl G (2009) Processing and properties of graded ceramic filters. J Am Ceram Soc 92:2854–2860
32. Anderson LE (1951) Filter element and method of making the same. US Patent 2,539,768
33. Dickerson D, Monnin M, Rickle G, Borer M, Stuart J, Velu Y, Haberkamp W, Graber J (2006) Gradient density depth filtration system. US Patent App. 11/140,801
34. Vida-Simiti I, Jumate N, Moldovan V, Thalmaier G, Sechel N (2012) Characterization of gradual porous ceramic structures obtained by powder sedimentation. J Mater Sci Technol 28:362–366
35. Dalwadi MP, Bruna M, Griffiths IM (2016) A multiscale method to calculate filter blockage. J Fluid Mech 809:264–289
36. Probstein RF (2005) Physicochemical hydrodynamics: an introduction. Wiley, Chichester
37. Taylor GI (1953) Dispersion of soluble matter in solvent flowing slowly through a tube. Proc R Soc Lond Series A 219:186–203

38. Field RW, Pearce GK (2011) Critical, sustainable and threshold fluxes for membrane filtration with water industry applications. Adv Colloid Interface Sci 164:38–44
39. Herterich JG, Xu Q, Field RW, Vella D, Griffiths IM (2017) Optimizing the operation of a direct-flow filtration device. J Eng Math 104:195–211
40. Giglia S, Straeffer G (2012) Combined mechanism fouling model and method for optimization of series microfiltration performance. J Membr Sci 417:144–153
41. Griffiths I, Kumar A, Stewart P (2014) A combined network model for membrane fouling. J Colloid Interface Sci 432:10–18
42. Miller DJ, Kasemset S, Paul DR, Freeman BD (2014) Comparison of membrane fouling at constant flux and constant transmembrane pressure conditions. J Membr Sci 454:505–515